ISSN 1674-1056
http://cpb.iphy.ac.cn
http://iopscience.iop.org/cpb
中国物理 B
Chinese Physics
中国物理
Chinese Physics B

# Theoretical study of the radiative decay processes in $H^+(D^+, T^+)$-Be collisions

Huilin Wei(魏惠琳), Xiaojun Liu(刘晓军)

**Citation:**Chin. Phys. B . 2018, 27(12): 123101. **doi:** 10.1088/1674-1056/27/12/123101
Journal homepage: http://cpb.iphy.ac.cn; http://iopscience.iop.org/cpb

**What follows is a list of articles you may be interested in**

---

## MRCI+Q study of the low-lying electronic states of CdF including spin—orbit coupling

Shu-Tao Zhao(赵书涛), Bing Yan(闫冰), Rui Li(李瑞), Shan Wu(武山), Qiu-Ling Wang(王秋玲)

Chin. Phys. B . 2017, 26(2): 023105. **doi:** 10.1088/1674-1056/26/2/023105

## Configuration interaction studies on the spectroscopic properties of PbO including spin—orbit coupling

Wang Luo(罗旺), Rui Li(李瑞), Zhiqiang Gai(盖志强), RuiBo Ai(艾瑞波), Hongmin Zhang(张宏民), Xiaomei Zhang(张晓美), Bing Yan(闫冰)

Chin. Phys. B . 2016, 25(7): 073101. **doi:** 10.1088/1674-1056/25/7/073101

## Spectroscopic properties and radiative lifetimes of SiTe：A high-level multireference configuration interaction investigation

Li Rui, Zhang Xiao-Mei, Jin Ming-Xing, Xu Hai-Feng, Yan Bing

Chin. Phys. B . 2014, 23(5): 053101. **doi:** 10.1088/1674-1056/23/5/053101

## *Ab initio* MRCI+Q study on potential energy curves and spectroscopic parameters of low-lying electronic states of $CS^+$

Li Rui, Wei Chang-Li, Sun Qi-Xiang, Sun Er-Ping, Jin Ming-Xing, Xu Hai-Feng, Yan Bing

Chin. Phys. B . 2013, 22(12): 123103. **doi:** 10.1088/1674-1056/22/12/123103

## Multireference calculations on low-lying states and $X^3\Pi_u$-$^3\Pi_g$ absorption spectra of indium dimer

Zhou Ling-Song, Yan Bing, Jin Ming-Xing

Chin. Phys. B . 2013, 22(4): 043102. **doi:** 10.1088/1674-1056/22/4/043102

---

# Theoretical study of the radiative decay processes in $H^+(D^+, T^+)$–Be collisions*

Huilin Wei(魏惠琳)[1] and Xiaojun Liu(刘晓军)[2,†]

[1] *Beijing Sport University, Beijing* 100084, *China*
[2] *Department of Physics, College of Science, Qiqihar University, Qiqihar* 161006, *China*

(Received 30 August 2018; revised manuscript received 10 October 2018; published online 10 November 2018)

The potential energy curves of $X^1\Sigma^+$, $A^1\Sigma^+$, $C^1\Sigma^+$, and $B^1\Pi$ are calculated with high-level MRDCI method, and the calculated spectroscopic constants of those states are in good agreement with most recent experimental data. On the basis of high precision PECs, the radiative processes of $H^+ +$ Be collisions are studied by using the fully quantum, optical potential and semiclassical methods in the energy ranges of $10^{-8}$ eV/u–0.1 eV/u, and the radiative decay, the radiative charge transfer, and the radiative association cross-sections are computed. It is found that the radiative association process is dominant in the energy region of $10^{-8}$ eV/u–0.02 eV/u, while radiative charge transfer becomes important at higher energies. Rich resonance structures are present in the radiative association and charge transfer cross-sections in the whole energy region considered, which result from the interaction between the quasi-bound rovibrational $(J, v)$ states in the entrance channel with the final continuum state. Significant isotope effects have been found in the radiative decay processes of $H^+ +$ Be collisions.

**Keywords:** optical-potential method, radiative charge transfer, radiative association, radiative decay, isotope effects

**PACS:** 31.50.Df, 31.15.aj, 31.15.ag **DOI:** 10.1088/1674-1056/27/12/123101

## 1. Introduction

As a rare light element, Beryllium is the lightest stable nuclide not synthesized in the Big Bang and it has been used as probe as formation of the early universe, Galactic evolution and stellar structure together with Li and B,[1–4] which are regarded as a pure product of cosmic-ray (CR) spallation nucleosynthesis, are produced only by the cannonade of $^{13}C$ and $^{16}O$ by protons and $\alpha$ -particles. The abundances of these light elements and the corresponding ratio supplies some meaningful information on the affection of a planetary companion in the formation and evolution of stars.[5–10] For fusion science, beryllium is treated as a primary wall material and hydrogen is treated as the main plasma constituent, hence, studies of the collision processes between beryllium and hydrogen are of great interest.[1] Since 2011, the JET experiment has been carried out through an ITER-like wall that is constituted of beryllium and tungsten. In a plasma environment, beryllium erodes very easily because of chemical and physical sputtering, which discharge $BeH_2$, BeH Be, and $Be^+$ into the environment. Therefore, in the edge and divertor region of fusion plasma devices, a large variety of atomic and molecular collision processes need to be taken into account in modeling and interpreting spectroscopic diagnostics.

As the simplest beryllium hydride, the electronic structures of BeH and $BeH^+$ have been intensively investigated by a number of research groups. A great number of methods have been constructed and used to calculate accurate potential energy curves (PECs) and spectroscopic constants. Colin *et al.* determined the Rydbcrg–Klein–Rees (RKR) potential energy curves of low-lying states ($X^2\Sigma^+$, $C^2\Sigma^+$, and $A^2\Pi$) of BeH via spectroscopy analysis.[11,12] Later, the spectroscopic constant of $X^2\Sigma^+$ were evaluated by Colin *et al.* using high resolution infrared emission spectra of BeH.[13] Le Roy *et al.*[14] determined a 'spectroscopic' PEC of BeH through extracting the previously available experimental results of Colin *et al.* A precise ground-state PEC of BeH was recently obtained by Koput[15] utilizing a high-level *ab initio* method. Pitarch *et al.*[16] used a full configuration interaction method to compute the PECs and dipole moment curves of the low-lying states of BeH, and the avoided crossing between the electronic states of the same symmetry are discussed. Pitarch *et al.*[17] also used the same method to calculate vertical excitation energies, transition dipole, quadrupole moments, and oscillator strengths, and the transition properties were illuminated. In 1982, the PECs and spectroscopic constants for the $X^1\Sigma^+$ and $A^1\Sigma^+$ were computed by Ornellas *et al.* using the configuration interaction method.[18] Subsequently, Ornellas *et al.* systematically investigated[19–22] of the PECs, dipole moment functions, transition dipole moment functions and radiative transition probabilities of rovibrational states of $BeH^+$. Recently, Bubin and Adamowicz[23] carried out Non–Born–Oppenheimer computations to obtain the ionization energy of BeH and dissocia-

*Project supported by the Natural Science Foundation of Heilongjiang Province of China (Grant No. A2015011) and the Scientific Research Plan Projects of Heilongjiang Educational Department, China (Grant No. 135209258).

†Corresponding author. E-mail: xiaojunliuqqhr@163.com

© 2018 Chinese Physical Society and IOP Publishing Ltd 

tion energies of BeH/BeH$^+$. Farjallah *et al.*[24] used the high-level quantum chemistry method, combining pseudo-potential to calculate the low-lying 44 electronic states of BeH$^+$.

Some studies have recently been reported for collision processes of Be$^+$–H and H$^+$–Be. Errea *et al.*[25] investigated the total cross-sections of excitation and charge transfer processes in Be$^+$–H or H$^+$–Be collisions in the energy range of 0.2 keV/u–25 keV/u by employing the semiclassical molecular orbital close-coupling approach (SMOCC). Krstić and Schultz calculated the elastic differential and integral cross-sections, momentum transfer and viscosity cross-sections in Be$^+$–H and H$^+$–Be collision processes by utilizing the quantum-mechanically approach and the classical trajectory Monte Carlo (CTMC)[26] approach. More recently, Liu *et al.* studied the elastic, momentum transfer and projectile excitation cross-sections in Be$^+$–H via the multichannel quantal molecular orbital close-coupling computations.[27] Compared with theoretical investigations, there are relatively few experimental work owing to the fact that BeH and BeH$^+$ are extremely poisonous. Vibration-rotation spectra of BeH$^+$ were investigated by different research groups.[13,28,29]

In this work, we conduct an extensive investigation on the radiative decay of H$^+$(D$^+$, T$^+$)–Be(2 s$^2$) collision processes in the energy range of $10^{-8}$ eV–$10^{-1}$ eV, including the radiative charge transfer:

$$\mathrm{H}^+(\mathrm{D}^+,\mathrm{T}^+)+\mathrm{Be}(2\mathrm{s}^2)\rightarrow \mathrm{H}(1\mathrm{s})+\mathrm{Be}^+(1\mathrm{s}^2 2\mathrm{s})+h\nu \quad (1)$$

and the radiative association processes

$$\mathrm{H}^+(\mathrm{D}^+,\mathrm{T}^+)+\mathrm{Be}(2\mathrm{s}^2)\rightarrow \mathrm{HBe}^+(1\mathrm{s}^2 2\mathrm{s})+h\nu, \quad (2)$$

in which the used adiabatic potential curves and dipole transition moment curves are computed by the multi-reference configuration interaction method (MRDCI).[30,31]

## 2. Method and computational details

In this work, the MRDCI procedure[30,31] is utilized to compute the PECs of the lowest three $^1\Sigma^+$ and the lowest $^1\Pi$ electronic state of BeH$^+$ molecular ion. All of the inner shell and valence shell electrons of BeH$^+$ molecular ion are considered in the MRDCI computations. The correlation consistent quadruple zeta Gaussian-type all-electron cc-pVQZ basis sets[33] are applied to describe beryllium and hydrogen atoms in the above calculations. In addition, the (3s, 3p, 3d) diffuse functions are included for the well-described Rydberg states. In the internuclear distances range of $1.5a_0$–$100a_0$, the threshold for electronic configuration composition of BeH$^+$ is chosen as $10^{-8}$ Hartree. With the aid of the Winger–Witmer principle, the corresponding relationship between electronic states and dissociation limits are presented as:

$$\mathrm{Be}^+(^2\mathrm{S_g})+\mathrm{H}(^2\mathrm{S_g})\rightarrow(^1\Sigma^+)+(^3\Sigma^+), \quad (3)$$

$$\mathrm{Be}^+(^2\mathrm{P_u})+\mathrm{H}(^2\mathrm{S_g})\rightarrow(^1\Sigma^++{}^1\Pi)+(^3\Sigma^++{}^3\Pi), \quad (4)$$

$$\mathrm{Be}(^1\mathrm{S_g})+\mathrm{H}^+(^1\mathrm{S_g})\rightarrow(^1\Sigma^+). \quad (5)$$

The calculated wave functions are then used to determine the dipole transition moments $D_{i,j}(R)$ required in scattering calculations:

$$D_{i,j}(R)=\int \Psi_i^*(r,R)\Big(\sum_k er_k\Big)\Psi_j(r,R)\,\mathrm{d}r, \quad (6)$$

in which $\Psi_i(r,R)$ and $\Psi_j(r,R)$ are the wave functions of the initial state $i$ and the final state $j$, respectively.

In this paper, the fully quantum-mechanical method has been applied for the treatment of the two radiative decay processes, radiative charge transfer and radiative association processes. In addition, both optical-potential and semiclassical methods have been adopted to study the radiative decay process for comparison. We will outline these methods in the following discussion.

### 2.1. Fully quantum-mechanical method for radiative charge transfer and radiative association

The total emission cross-section in the collision process is defined by the sum of two contributions from radiative charge transfer and radiative association processes. In this work, we apply the fully quantum-mechanical method to compute the radiative charge transfer cross-section[9,10] and radiative association cross-section.[15,17] Now, we will give a brief account of the method. The radiative charge transfer cross-section is formulated as

$$\sigma = \frac{8}{3}\left(\frac{\pi}{k_\mathrm{A}}\right)^2\int_{\omega_{\min}}^{\omega_{\max}}\frac{\omega^3}{c^3}\sum_J[JM^2_{J,J-1}(k_\mathrm{A},k_\mathrm{X}) + (J+1)M^2_{J,J+1}(k_\mathrm{A},k_\mathrm{X})]\,\mathrm{d}\omega, \quad (7)$$

where $c$ is the velocity of light, $\omega$ is the angular frequency of the released photon, $J$ is the quantum number of angular momentum, $k_\mathrm{A}$ is the initial momentum, $k_\mathrm{X}$ is the final momentum, and $M_{J',J}$ is the transition dipole moment between upper and lower states. The radiative association cross-section can be written as

$$\sigma=\frac{8}{3}\left(\frac{\pi}{k}\right)^2\sum_J\sum_v\frac{\omega^3}{c^3}[JM^2_{E,J-1;J,v}+(J+1)M^2_{E,J+1;J,v}], \quad (8)$$

where $k$ is the wave number, $J$ is the quantum number of rotational state, $v$ is the quantum number of vibrational state. The transition dipole moment $M_{J',J}$ can be represented by the two energy-normalized continuum wave functions $f_{J'}(R)$ and $\phi_J^n(R)$

$$M_{J',J}=\int_0^\infty \mathrm{d}R f_{J'}(R)D(R)\phi_J^n(R). \quad (9)$$

Here $D(R)$ is the dipole transition matrix element, $R$ is the internuclear distance.

The entrance and exit wave function are obtained by solving the homogeneous radial equations

$$\left\{\frac{\mathrm{d}^2}{\mathrm{d}R^2}-\frac{J(J+1)}{R^2}-\frac{2\mu}{\hbar^2}\left[V_{\mathrm{A}}(R)-V_{\mathrm{A}}(\infty)\right]+k^2\right\}f_{J'}(R)=0,$$
$$\left\{\frac{\mathrm{d}^2}{\mathrm{d}R^2}-\frac{J'(J'+1)}{R^2}-\frac{2\mu}{\hbar^2}\left[V_{\mathrm{X}}(R)-V_{\mathrm{X}}(\infty)\right]-E_{n,J}\right\}\phi_J^n(R)=0. \tag{10}$$

Here $\mu$ is the reduced mass, $V_{\mathrm{A}}(R)$and $V_{\mathrm{X}}(R)$ are the PEC of the entrance and exit states, here $E_{n,J}=E+\Delta E-\hbar\omega$, $E$ is the relative collision energy of the initial particle in the center-of-mass frame, $\Delta E$ is the difference of transition energy.

The normalized asymptotical continuum wave functions is given by

$$f_{J'}(R)=\sqrt{\frac{2\mu}{\hbar^2\pi k}}\sin\left(kR-\frac{J'\pi}{2}+\delta_{J'}\right), \tag{11}$$

where $\delta_{J'}$ is the phase shift.

### 2.2. Optical-potential and semiclassical methods for radiative decay

The total radiative decay cross-sections are evaluated with the optical potential approach.[9,10] In the processes of the ion-atom collisions, the transition probability is expressed by the imaginary part of a complex optical potential. The scattering wave $F_{\mathrm{A}}(\boldsymbol{R})$ is obtained by solution of the Schrödinger equation

$$\left[-\frac{1}{2\mu}\nabla^2_{\boldsymbol{R}}+V_{\mathrm{A}}(\boldsymbol{R})-E\right]F_{\mathrm{A}}(\boldsymbol{R})=\frac{\mathrm{i}}{2}A(R)F_{\mathrm{A}}(\boldsymbol{R}), \tag{12}$$

where subscript A denotes the initial upper molecular state, $E$ is the collision energy in the entrance channel, and $A(R)$ is the transition probability for the radiative transition determined by

$$A(R)=\frac{4}{3}D^2(R)\frac{|\Delta E(R)|^3}{c^3}, \tag{13}$$
$$\Delta E(R)=V_{\mathrm{A}}(R)-V_{\mathrm{X}}(R), \tag{14}$$

where $V_{\mathrm{A}}(R)$ and $V_{\mathrm{X}}(R)$ are the adiabatic potential energy for the upper and lower states, respectively. $D(R)$ is the dipole transition matrix element between the states A and X.

The radiative-decay cross-sections are determined by

$$\sigma(E)=\frac{\pi}{k_{\mathrm{a}}^2}\sum_J^{\infty}(2J+1)[1-\exp(-4\eta_J)] \tag{15}$$

and the $\eta_J$ represents the imaginary part of the phase shift for the $J$-th partial wave of the radial Schrödinger equation, which is obtained from the distorted-wave approximation[9,10] as

$$\eta_J=\frac{\pi}{2}\int_0^{\infty}\mathrm{d}R\,|f_J^{\mathrm{a}}(k_{\mathrm{a}}R)|^2A(R) \tag{16}$$

where $k_{\mathrm{a}}$ is given by

$$k_{\mathrm{a}}=\sqrt{2\mu[E-V_{\mathrm{a}}(\infty)]}. \tag{17}$$

To investigate radiative decay of higher energies, substituting the summation in Eq. (15) and adopting the Jeffreys–Wentzel–Kramers–Brillouin (JWKB) approximation, one determines the formula for the semiclassical cross-section

$$\sigma(E)=2\pi\left(\frac{2\mu}{E}\right)^2\int p\,\mathrm{d}p\int_{R_{\mathrm{a}}^{\mathrm{ctp}}}^{\infty}\mathrm{d}R \times\frac{A(R)}{(1-V_{\mathrm{a}}(R)/E-p^2/R^2)^{1/2}}, \tag{18}$$

where $p$ represents the impact parameter, and $R_{\mathrm{a}}^{\mathrm{ctp}}$ represents the classical turning point of the incoming channel.[10] This formula has been employed to compute a series of cross-sections of the radiative process. For energy range ($E\geq V_{\mathrm{a}}$), the double integral is almost energy independent, hence, $\sigma(E)$ changes as $E^{-1/2}$.

## 3. Results and discussion

### 3.1. Molecular structure calculations and dipole transition moments

In Fig. 1, the calculated adiabatic energies of lowest 3 $^1\Sigma^+$ and 1 $^1\Pi$ electronic states are only presented in the interval of internuclear distances $1.5a_0$–$20a_0$ for visual clarity. These four electronic states are associated with three dissociation limits $\mathrm{Be}^+(^2\mathrm{S_g})+\mathrm{H}(^2\mathrm{S_g})$, $\mathrm{Be}^+(^2\mathrm{P_u})+\mathrm{H}(^2\mathrm{S_g})$, and $\mathrm{Be}(^1\mathrm{S_g})+\mathrm{H}^+(^1\mathrm{S_g})$. Since we only study rovibrational transition between the singlet electronic states, the PECs of 1-2 $^3\Sigma^+$ and 1 $^3\Pi$, correlated with dissociation limit $\mathrm{Be}^+(^2\mathrm{S_g})+\mathrm{H}(^2\mathrm{S_g})$ and $\mathrm{Be}^+(^2\mathrm{P_u})+\mathrm{H}(^2\mathrm{S_g})$, are omitted in this paper. For the convenience of applications, the spectroscopic parameters of bound states are obtained from the numerical PECs, including the adiabatic transition energy ($T_{\mathrm{e}}$), the harmonacity frequency ($\omega_{\mathrm{e}}$), the anharmonacity frequency ($\omega_{\mathrm{e}}x_{\mathrm{e}}$), the rotational constant ($B_{\mathrm{e}}$), the equilibrium distance ($R_{\mathrm{e}}$), and the dissociation energy ($D_{\mathrm{e}}$). These calculated spectroscopic constants are presented in Table 1 in comparison with previously available experimental and theoretical results, which serve as the universal method to check the precise of theoretical calculation.

As can be seen in Table 1, there is a good agreement between our work, the experimental works and the theoretical calculations. For the ground state $X^1\Sigma^+$, the well depth of the state is computed to be 3.20 eV, which differs by 0.06 eV (1.8%) from available experiment.[29] Good agreement with the experiments for other spectroscopic constants is also obtained. It is found $R_{\mathrm{e}}=2.477$ a.u., $\omega_{\mathrm{e}}=2228.6\ \mathrm{cm}^{-1}$, $\omega_{\mathrm{e}}x_{\mathrm{e}}=40.07\ \mathrm{cm}^{-1}$, and $B_{\mathrm{e}}=10.8285\ \mathrm{cm}^{-1}$, which agree well with those obtained by Herzberg[28] ($R_{\mathrm{e}}=2.479$ a.u., $\omega_{\mathrm{e}}=2221.7\ \mathrm{cm}^{-1}$, $\omega_{\mathrm{e}}x_{\mathrm{e}}=39.79\ \mathrm{cm}^{-1}$, and $B_{\mathrm{e}}=10.80\ \mathrm{cm}^{-1}$). The differences of $R_{\mathrm{e}}$, $\omega_{\mathrm{e}}$, $\omega_{\mathrm{e}}x_{\mathrm{e}}$, and $B_{\mathrm{e}}$ between our results and Herzberg's data are 0.002 (0.1%), 6.9 $\mathrm{cm}^{-1}$ (0.3%), 0.28 $\mathrm{cm}^{-1}$ (0.7%), and 0.0285 $\mathrm{cm}^{-1}$ (0.3%). There is an excellent agreement between our work and those of Farjallah *et*

*al.*,[24] Machado and Ornellas,[22] and Ornellas,[18] but the differences become larger in comparison with the calculations of Banyard and Taylor.[34] For the first excited state $A^1\Sigma^+$, our calculated $R_e$, $T_e$, $D_e$ data are in good agreement with the latest experimental data of Coxon and Colin[29] and the theoretical results of Ornellas.[18] For the excited states of $B^1\Pi$ and $C^1\Sigma^+$, no measurement data available; however, the present results accord with the existing theoretical data of Machado and Ornellas[22] and Farjallah.[24]

The dipole transition moments between singlet states are computed with MRDCI method, and dipole transition moments along the internuclear distance are presented in Fig. 2. It can be found that the dipole transition moments of X–A and X–B become constant at large internuclear distance, while other dipole transition moment of X–C approach to zero at dissociation limit. The variation of the dipole transition moment between singlet states can be explained by the permanent dipole transition moment between $Be^+(2s)$ and $Be^+(2p)$, which is correlated with the asymptotic low-lying states of X and A & B, respectively.

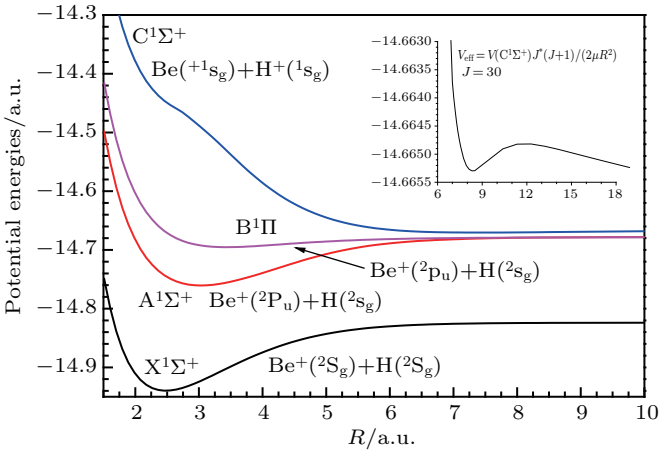



**Fig. 1.** (color online) MRDCI potential energy curves for $BeH^+$ along with internuclear distance $R$. Note that the inset is the effective potential energy curve of $V_J^{\rm eff}(R) = V(R) + J(J+1)/2\mu R^2$ of the state $C^1\Sigma^+$ with $J = 30$ as an example. The unit a.u. is short for atomic unit.

**Table 1.** Spectroscopic constants for the low-lying bound states of $BeH^+$.

| Electronic state | Ref. | $r_e$/a.u. | $\omega_e$/cm$^{-1}$ | $\omega_e x_e$/cm$^{-1}$ | $B_e$/cm$^{-1}$ | $T_e$/cm$^{-1}$ | $D_e$/eV |
|---|---|---|---|---|---|---|---|
| $X^1\Sigma^+$ | this work | 2.477 | 2228.6 | 40.07 | 10.8285 | 0 | 3.20 |
| | [29] | 2.476 | | | | 0 | 3.26 |
| | [28] | 2.479 | 2221.7 | 39.79 | 10.80 | 0 | 3.28 |
| | [18] | 2.473 | 2243.1 | 40.19 | 10.862 | 0 | 3.38 |
| | [22] | 2.479 | 2221.6 | 40.16 | 10.805 | 0 | 3.38 |
| | [24] | 2.470 | 2256.1 | 43.12 | 10.88 | 0 | 3.32 |
| | [19] | 2.487 | 2227.3 | 39.1 | 10.732 | 0 | 2.65 |
| | [34] | 2.52 | 2146 | 40 | 10.42 | 0 | 3.07 |
| $A^1\Sigma^+$ | this work | 3.022 | 1494.4 | 20.00 | 7.2753 | 39320 | 2.28 |
| | [29] | 3.034 | | | | 39416 | 2.33 |
| | [28] | 3.041 | 1476.1 | 14.80 | 7.184 | | 2.02 |
| | [18] | 3.030 | 1468.0 | 14.05 | 7.232 | | 2.32 |
| | [22] | 3.031 | 1481.7 | 14.69 | 7.231 | 39 307 | 2.20 |
| | [24] | 3.000 | 1464.9 | 18.31 | 7.45 | 39 025 | 2.31 |
| $C^1\Sigma^+$ | this work | 7.0775 | 335.0 | 7.17 | 1.23908 | 59514 | 0.13 |
| | [24] | 8.01 | 193.53 | 7.09 | 1.0359 | 60304 | 0.10 |
| $B^1\Pi$ | this work | 3.421 | 872.3 | 48.72 | 5.6933 | 53819 | 0.48 |
| | [22] | 3.437 | 869.5 | 50.32 | 5.621 | 53 753 | 0.44 |
| | [24] | 3.400 | 834.8 | 55.63 | 5.760 | 54 091 | 0.47 |

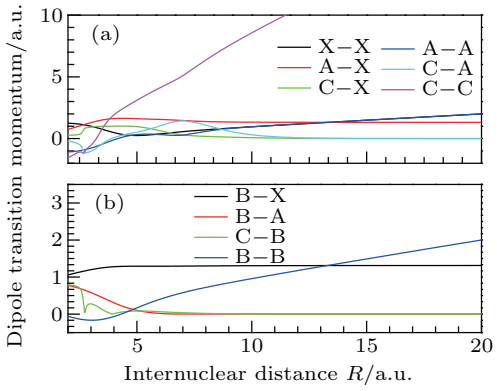



**Fig. 2.** (color online) Calculated MRDCI dipole transition moment for $BeH^+$ along with internuclear distance $R$.

### 3.2. Radiative cross-section and isotope effects

The results of present calculations for the processes (1) and (2), including the radiative decay, radiative charge transfer and radiative association cross-sections, are shown in Figs. 3(a), 3(b), and 3(c). Since the radiative decay processes only become important at very low energy collisions, these collision radiative cross-sections are computed and presented in the energy range of $E = 10^{-8}$ eV/u–$10^{-1}$ eV/u, which are the typical energy range in the astrophysics studies. In Fig. 3(a), Fig. 3(b), and Fig. 3(c), the radiative decay, radiative charge transfer and radiative association cross-sections are presented for $H^+$–Be, $D^+$–Be, and $T^+$–Be collisions, where

similar results can be observed both on magnitudes and structures. In the following, we will discuss the Fig. 3(a) in detail for $H^+$–Be collisions, as an example. For $D^+$–Be and $T^+$–Be collisions, all the analysis and discussions are applicable.

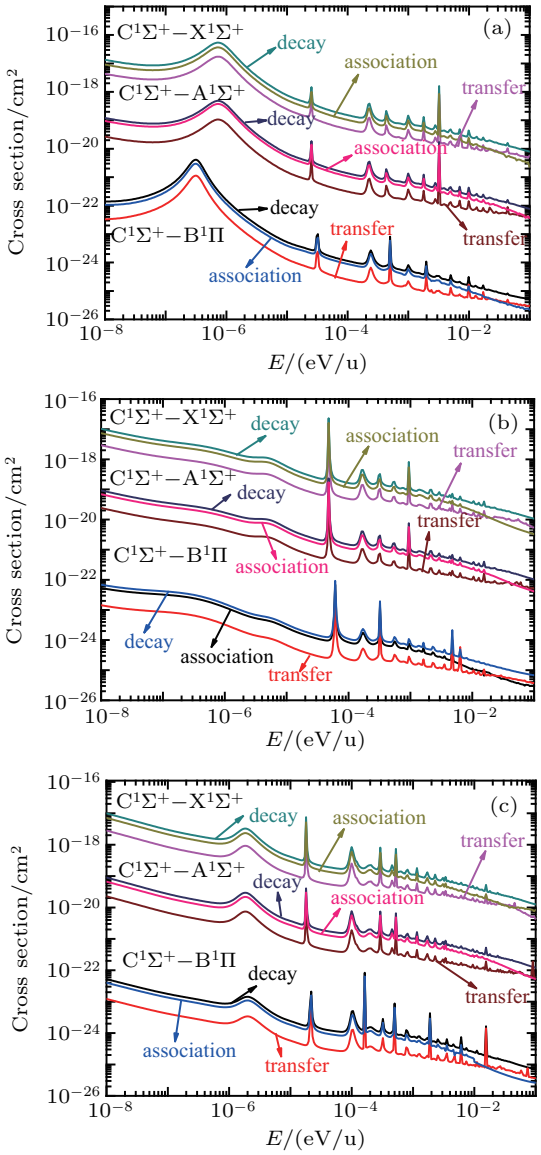



**Fig. 3.** (color online) (a) The radiative decay, radiative charge transfer, and radiative association cross-sections of $C^1\Sigma^+$–$X^1\Sigma^+$, $C^1\Sigma^+$–$A^1\Sigma^+$, $C^1\Sigma^+$–$B^1\Pi$ transitions in $H^+$–Be collisions. (b) The radiative decay, radiative charge transfer, and radiative association cross-sections of $C^1\Sigma^+$–$X^1\Sigma^+$, $C^1\Sigma^+$–$A^1\Sigma^+$, $C^1\Sigma^+$–$B^1\Pi$ transitions in $D^+$–Be collisions. (c) The radiative decay, radiative charge transfer, and radiative association cross-sections of $C^1\Sigma^+$–$X^1\Sigma^+$, $C^1\Sigma^+$–$A^1\Sigma^+$, $C^1\Sigma^+$–$B^1\Pi$ transitions in $T^+$–Be collisions.

In Fig. 3(a), it can be found that all the radiative cross-sections decrease with the increase of incident energy $E$, behaving as $E^{-1/2}$ and varying approximately as the Langevin cross-section formula for a polarization potential for incident energy less than $10^{-2}$ eV/u. In comparing the radiative cross-sections for the $C^1\Sigma^+$–$X^1\Sigma^+$, $C^1\Sigma^+$–$A^1\Sigma^+$, and $C^1\Sigma^+$–$B^1\Pi$ transitions, it can be found that the first is dominant, about two and five orders larger than the second and third, respectively. The differences are caused by the large difference of the Einstein coefficients, which are determined by the adiabatic potentials and the dipole transition moments between these states. For the radiative transitions of $C^1\Sigma^+$–$X^1\Sigma^+$, $C^1\Sigma^+$–$A^1\Sigma^+$, and $C^1\Sigma^+$–$B^1\Pi$, two interesting features can be observed: the first is that the radiative association processes dominate corresponding radiative decay processes in the lower energy range; and the second is that for the radiative decay, radiative charge transfer and radiative association cross-sections, there are similar oscillation structures present. Interestingly, the distinct peaks in these structures locate at the same energies.

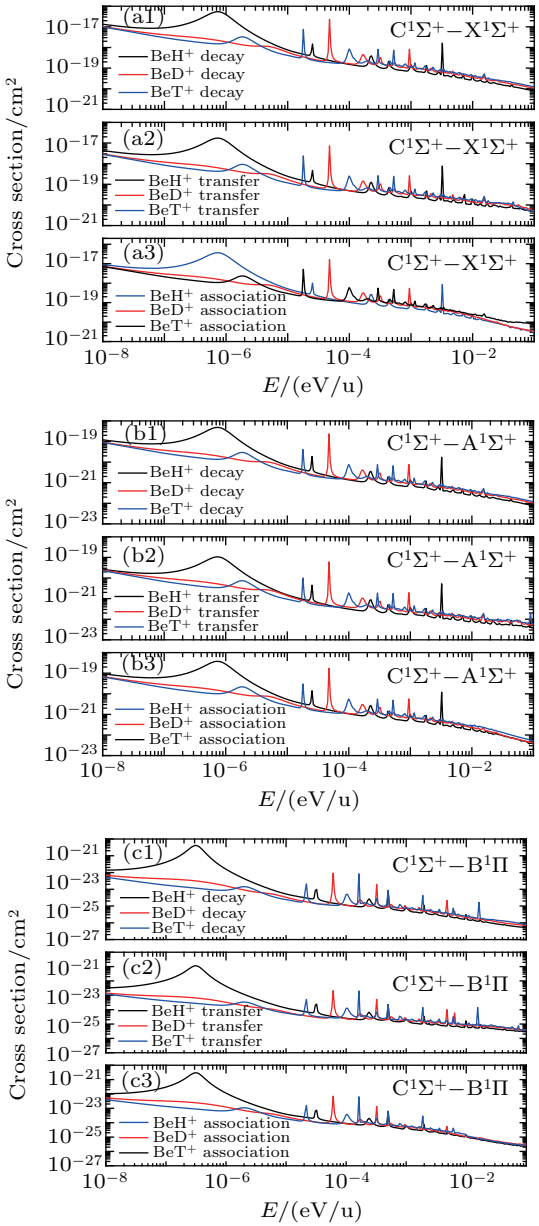



**Fig. 4.** (color online) (a1)–(a3) The radial decay, radial charge transfer, and radial association cross-sections for the $C^1\Sigma^+$–$X^1\Sigma^+$ channel of $BeH^+$, $BeD^+$, and $BeT^+$. (b1)–(b3) The radial decay, radial charge transfer, and radial association cross-sections for the $C^1\Sigma^+$–$A^1\Sigma^+$ channel of $BeH^+$, $BeD^+$, and $BeT^+$. (c1)–(c3) The radial decay, radial charge transfer, and radial association cross-sections for the $C^1\Sigma^+$–$B^1\Pi$ channel of $BeH^+$, $BeD^+$, and $BeT^+$.

In the collisions complex of $H^+$($D^+$, $T^+$)–Be, there are obvious wells $D_e$ for $X^1\Sigma^+$, $A^1\Sigma^+$, and $B^1\Pi$ states, which are

3.20 eV, 2.28 eV, and 0.48 eV, respectively, as shown in Table 1. For these deep potential wells, large number of molecular bound rovibrational states will come into being. Therefore, molecular ions are easy to form with a deep well presented ion-atom collisions at very low collision energy. For the case of radiative collisions, molecular ions will be formed after collisions with an emitted photon; namely, the radiative association processes. With the increase of the incident energy or in the case of shallow well depth, the bound molecular ions are difficult to form and the continuum states become dominant. Correspondingly, the radiative charge transfer processes become dominant in ion-atom collisions.

For these resonance structures, appearing in the energy region of $10^{-6}$ eV/u–$10^{-1}$ eV/u, are attributed to the presence of some specific rovibrational levels ($v'$, $J'$) in the entrance channel,[35–37] as shown in Fig. 1. It can be found that there is a potential barrier due to the contributions from the centrifugal term, which causes some quasibound or virtual rovibrational states and produces these resonance structures. Therefore, all of the collision radiative cross-sections for $C^1\Sigma^+$–$X^1\Sigma^+$, $C^1\Sigma^+$–$A^1\Sigma^+$, and $C^1\Sigma^+$–$B^1\Pi$, transitions in $H^+$–Be collisions present same oscillations structures and each resonance states result from the same rovibrational state.

Significant isotope effects have been observed in low-energy non-radiative processes in ion-atom/molecule collisions,[38] it is interesting to see whether the isotope effects are important in the collision radiative processes. As shown in Figs. 4(a), 4(b), and 4(c), the radiative cross-sections for $C^1\Sigma^+$–$X^1\Sigma^+$, $C^1\Sigma^+$–$A^1\Sigma^+$, and $C^1\Sigma^+$–$B^1\Pi$ are presented, respectively, for comparison between $H^+$–Be, $D^+$–Be, and $T^+$–Be collisions. Similarly, the $C^1\Sigma^+$–$X^1\Sigma^+$ transitions in Fig. 4(a) will be discussed in detail, and all analysis and conclusions hold for $C^1\Sigma^+$–$A^1\Sigma^+$ and $C^1\Sigma^+$–$B^1\Pi$ transitions.

In Fig. 4(a), it can be found that the radiative cross-sections increase with the increase of reduced mass at the higher energy side, but a different tendency is observed at the low energy side. For example, the ratio of the cross-sections of $D^+$–Be to $H^+$–Be is about 1.35 at the energy of 0.1 eV/u in Fig. 4 and the one of $T^+$ to $H^+$ cross-sections is about 1.57. Unlike the case of non-radiative collision process, the isotope effects in the radiative processes in $H^+$ ($D^+$, $T^+$)–Be collisions are mainly attributed to the kinematic isotope effects due to the different reduce masses of collision complex ($HBe^+$, $DBe^+$, and $TBe^+$), and are not related to the radial or rotational couplings, which are the main mechanism causing isotope effects in non-radiative processes in low-energy ion-atom/molecule collisions.

## 4. Conclusions

Accurate PECs of singlet states of $BeH^+$ are computed using the MRDCI method. The spectroscopic constants of $X^1\Sigma^+$, $A^1\Sigma^+$, $C^1\Sigma^{+-}$, and $B^1\Pi$ states are evaluated, and agree well with previous experimental data. On the basis of high precision PECs, the radiative association, radiative charge transfer and radiative decay cross-sections for the $H^+/D^+/T^+ + Be$ collisions in energy of $10^{-8}$ eV/u–0.1 eV/u are evaluated using the fully quantum, optical potential and semiclassical approaches. It is found that the radiative association process is dominant in the very low energy range around $10^{-8}$ eV/u–0.02 eV/u and the radiative charge transfer process becomes more important for higher energies. Moreover, there are rich resonance structures in the collision radiative cross-sections in the energy range considered, which are produced from the interaction between the quasi-bound rovibrational $(J, v)$ states of the initial channel with the continuum state of the final channel. Isotope effects have been observed in the radiative decay processes, which are attributed to the kinematic effects due to the differences of the reduced masses of the collision complex and cannot be neglected in ion–atom collisions.

## References


[1] Lambert D 1993 *Phys. Scr.* **T47** 186
[2] Carlsson M, Rutten R J, Bruls J H M J and Shchukina N G 1994 *A. & A.* **288** 860
[3] Lyublinski I E and Vertkov A V 2010 *Fusion. Eng.* **85** 924
[4] Apicella M L, Mazzitelli G, Pericoli R V, Lazarev V, Alekseyev A, Vertkov A and Zagórski R 2007 *J. Nucl. Mater.* **363** 1346
[5] Sun E P, Ren T Q, Liu Q X, Miao Q, Zhang J J, Xu H F and Yan B 2016 *Chin. Phys. Lett.* **33** 023101
[6] Liu X M, Song Y H, Jiang W and Jia W Z 2018 *Chin. Phys. Lett.* **35** 45202
[7] Wu D, Lin C, Wen Y, Xie A and Yan B 2018 *Chin. Phys. B* **27** 083101
[8] Zuo W L, Lv H, Liang H J, Shan S M, Ma R, Yan B and Xu H F 2018 *Chin. Phys. B* **27** 063301
[9] Stancial P C and Zygelman B 1996 *Astrophys. J.* **472** 102
[10] Zygelman B and Dalgarno A 1988 *Phys. Rev. A* **38** 1877
[11] Colin R, Dreze C and Steinhauer M 1983 *Can. J. Phys.* **61** 641
[12] Focsa C, Firth S, Bernath P F and Colin R 1998 *J. Chem. Phys.* **109** 5795
[13] Shayesteh A, Tereszchuk K, Bernath P F and Colin R 2003 *J. Chem. Phys.* **118** 1158
[14] Le Roy R J 2002 *LEVEL* 7.5: a Computer Program for Solving the Radial Schrödinger Equation for Bound and Quasibound Levels
[15] Koput J 2011 *J. Chem. Phys.* **135** 244308
[16] Pitarch R J, Sánchez M J, Velasco A M and Martin I 2008 *J. Chem. Phys.* **129** 054310
[17] Pitarch R J, Sánchez M J and Velasco A M 2008 *J. Comput. Chem.* **29** 523
[18] Ornellas F R 1982 *J. Phys. B: At. Mol. Phys.* **15** 1977
[19] Ornellas F R 1983 *J. Mol. Struct.* **92** 337
[20] Ornellas F R, Stwalley W C and Zemke W T 1983 *J. Chem. Phys.* **79** 5311
[21] Ornellas F R 1985 *J. Chem. Phys.* **82** 379
[22] Machado F B C and Ornellas F R 1991 *J. Chem. Phys.* **94** 7237
[23] IBubin S and Adamowicz L 2007 *J. Chem. Phys.* **126** 214305
[24] Farjallah M, Ghanmi C and Berriche H 2013 *Eur. Phys. J. D* **67** 1

[25] Errea L F, Herrero B, Mhdez L, Rabadan I and Sanchez P 1994 *J. Phys. B: At. Mol. Opt. Phys.* **27** L753
[26] Krstić P S and Schultz D R 2009 *J. Phys. B: At. Mol. Opt. Phys.* **42** 065207
[27] Liu C H, Wang J G and Janev R K 2010 *J. Phys. B: At. Mol. Opt. Phys.* **43** 144006
[28] Huber K P and Herzberg G 1979 *Molecular Spectra and Molecular Structure IV, Constants of Diatomic Molecules* (New York: Van Nostrand-Reinhold)
[29] Coxon J A and Colin R 1997 *J. Mol. Spectrosc.* **181** 215
[30] Buenker R J and Phillips R A 1985 *J. Mol. Struct. Theochem.* **123** 291
[31] Krebs S and Buenker R J 1995 *J. Chem. Phys.* **103** 5613
[32] Dunning T H 1989 *J. Chem. Phys.* **90** 1007
[33] Mitroy J 2010 *Phys. Rev. A* **82** 052516
[34] Banyard K E and Taylor G K 1975 *J. Phys. B: At. Mol. Phys.* **8** L137
[35] Yan L L, Li X Y, Wu Y, Wang J G and Qu Y Z 2014 *Phys. Rev. A* **90** 032714
[36] He B, Liu L, Wang J J, Ding D and Zhang C H 2009 *Acta Phys. Sin.* **58** 8419 (in Chinese)
[37] Ding D, He B, Qu S X and Wang J G 2013 *Acta Phys. Sin.* **62** 033401 (in Chinese)
[38] Stancil P C and Zygelman B 1995 *Phys. Rev. Lett.* **75** 1495